Evanescent absorption in kinematic surface Bragg diffraction

H. Dosch*
School of Applied and Engineering Physics and Cornell High Energy Synchrotron Source (CHESS), Cornell University, Ithaca, New York 14853
(Received 27 June 1986)

The Bragg scattering excited under the conditions of total external reflection is discussed within a kinematic approach based on the distorted-wave approximation. Due to evanescent absorption at grazing angles the maximum of the interference function of the surface Bragg reflection is displaced into the vacuum by an amount determined by the mean electron density of the medium. X-ray scattering experiments performed on a mosaic single crystal with synchrotron radiation confirm the predictions of the kinematic theory and indicate the potential for obtaining structural information on the first atomic layers.

INTRODUCTION

Since the first experimental report on grazing-incidence diffraction (GID) by Marra and Eisenberger[1] a variety of applications of this method for the investigation of surface structures has emerged in the literature.[2–5] Most of the systems analyzed by these authors share the fact that the structure of the investigated top layers are distinctly different from the subsequent atomic layers, e.g., in the case of reconstructed single-crystal surfaces which have been studied extensively by Robinson[3] and others.[4,5] By employing the scheme of GID, where the penetration depth of the x rays remains small, the two-dimensional surface Bragg scattering ("Bragg rods") can be significantly *enhanced* with respect to the bulk Bragg scattering ("Bragg spots").

In this paper we will focus on the experimental aspects of the more complicated case, where the crystal surface does not exhibit a noticeable difference in the crystal structure, and where accordingly the feasibility of the experimental *separation* of the surface signal from the bulk signal is not at all evident *a priori*. We will show, however, that information on the first atomic layers is obtainable by the exploitation of total external reflection of the x rays in combination with an independent control of the incidence and exit angle of the x rays ("depth-controlled GID").[6]

The field of x-ray diffraction with simultaneous total external reflection has been discussed theoretically by Vineyard,[7] Dietrich and Wagner,[8,9] Cowan[10] and Afans'ev and Melkonyan[11] within different approaches encompassing the range from dynamic to kinematic scattering theory. The interpretation of the scattering phenomena observed in this study is based on a semikinematic approach, first conceived by Vineyard,[7] which will allow a particularly straightforward analysis of the experimental scattering intensities in terms of evanescent absorption effects. We will show, in what follows, that due to the evanescent absorption associated with total external reflection, the Bragg scattering excited under these conditions is characteristically altered from the conventional (bulk) scattering, and will demonstrate these effects in a synchrotron x-ray scattering experiment.

THEORY

The average index of refraction (n) is the fundamental quantity which controls the "optical effects" associated with grazing incidence diffraction. For an electromagnetic wave of frequency ν in a medium with resonances ν_i (of oscillator strength f_i) n has the general form

$$n_\nu = 1 + (\bar{\rho}_e e^2)/(2\pi m) \sum_i f_i/(\nu_i^2 - \nu^2) ,$$

where $\bar{\rho}_e$ is the mean electron density and m,e the electronic mass and charge, respectively. In the case of x rays, where ν is in general much larger than any resonance ν_i, the index of refraction then becomes

$$n_\infty = 1 - \lambda^2 \frac{\bar{\rho}_e r_e}{2\pi} \equiv 1 - \delta \tag{1}$$

and is thus slightly less than 1. Subsequently, total external reflection from a crystal surface occurs, when the incident electromagnetic field with wave vector $|k_i| = 2\pi/\lambda$ hits the surface under an angle α_i less than the critical angle $\alpha_c = \lambda(r_e \bar{\rho}_e/\pi)^{1/2}$. Values of α_c range from 3 to 5 mrad for typical x-ray wavelengths ($\sim$1 Å). In the above expression $r_e = e^2/mc^2 = 2.82 \times 10^{-5}$ Å is the classical electron radius and $\lambda = c/\nu$ the wavelength of the incident radiation (c is the velocity of light).

In the regime of total external reflection a specularly reflected intensity occurs, while inside the less dense medium the electromagnetic field decays exponentially within the penetration depth

$$l^* = \lambda/[2\pi(2\delta - \sin^2\alpha_i)^{1/2}] \tag{2}$$

which takes on values of typically 50 Å ("evanescent waves"). The intensities of the refracted and reflected waves and the phase relation between them and the incident wave field are described by the Fresnel coefficients of transmission (T) and reflection (R). The reflectivity

$|R|^2$ determines the specularly reflected intensity which is not considered in this study, whereas the transmissivity $|T|^2$ governs in particular the intensity deposited in the evanescent wave field. For a detailed discussion of the Fresnel coefficients we refer the reader to the textbook by Born and Wolf.[12] A summarizing discussion of T and R is also found in the papers by Vineyard[7] and by Dietrich and Wagner.[9] We focus here to the relevant case (which is realized in the experiment described below) of an incident electromagnetic field which is polarized perpendicular to the plane of incidence (see also Fig. 5 in the experimental section), then the corresponding transmission coefficient is (for a transparent medium)

$$T_i = \frac{2\sin\alpha_i}{\sin\alpha_i + (\sin^2\alpha_i - 2\delta)^{1/2}} \,. \tag{3a}$$

The solid line in Fig. 1 shows $|T_i|^2$ as a function of α_i/α_c: For $\alpha_i = 0$ the incident and specular wave fields are in counter-phase at the crystal surface leading to a zero intensity in the evanescent wave field ($|T_0|^2 = 0$), whereas for $\alpha_i = \alpha_c$, the phases of the two external waves match at the surface allowing the maximum evanescent field "leaking" into the less dense medium ($|T_c|^2 = 4$). In practice, however, one has to account for a nonzero photoelectric absorption affecting T_i (as well as R) essentially in the vicinity of the critical angle. By way of example we have calculated $|T_i|^2$ for the real systems Fe_3Al and Pb [including their linear absorption coefficients $\mu(Fe_3Al) = 1000\ cm^{-1}$ and $\mu(Pb) = 2500\ cm^{-1}$; dashed and dotted lines in Fig. 1],[13] illustrating that for absorbing materials the evanescent intensity may differ substantially at the critical angle from its ideal value. In a very good approximation the relation[13]

$$|T_c|^2 = \frac{4}{1 + 2\sqrt{\beta}/a_c} \tag{3b}$$

holds for the transmissivity at the critical angle and can be used in any practical case to calculate the maximum of the evanescent intensity.

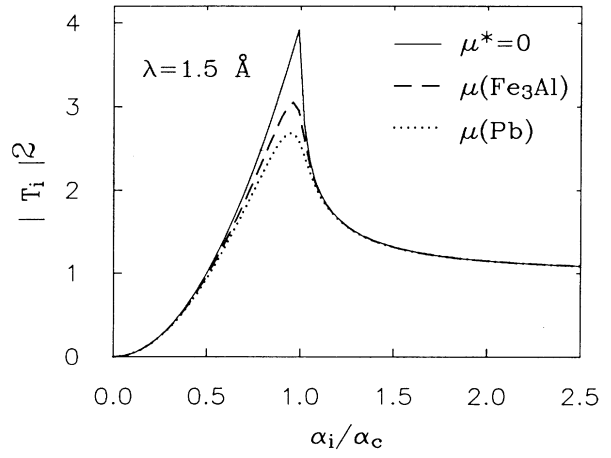

FIG. 1. Fresnel transmissivity $|T_i|^2$ as a function of α_i/α_c for a transparent medium and the real systems Fe_3Al and Pb.

In the kinematic scattering theory multiple scattering is neglected or, in other words, the x-ray index of refraction n is assumed to be exactly 1. Thus, a description of grazing incidence diffraction within the framework of the conventional kinematic theory cannot account for the strong optical effects in this regime, however, a pseudo-kinematic description of the scattering phenomena can somewhat be retained, if the evanescent wave field inside the medium ("distorted wave") is taken as the primary wave field instead of the (usually considered) incident wave field in the vacuum ("distorted-wave approximation," DWA).[7] Based on the DWA we will discuss in the following some significant properties of the GID Bragg interference function.

To begin with we want to point out that there are basically two different scattering geometries which allow the observation of Bragg scattering excited under conditions of total reflection (Fig. 2). In the case depicted in Fig. 2(a) the Bragg planes hkl (with a lattice spacing d_{hkl}) have a nonzero angle ϕ with respect to the crystal surface. Through the special choice of an x-ray wavelength $\lambda_\phi = 2d_{hkl}\sin\phi$, one can achieve that the incident wave vector $|k_i| = 2\pi/\lambda_\phi$ is forced to grazing angles $\alpha_i \leq \alpha_c$. Note that the angle α_f between the scattered wave k_f and the crystal surface is then close to 2ϕ which leads to a very asymmetric scattering geometry. (This experimental

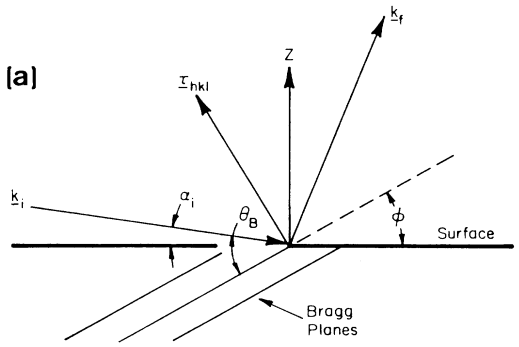

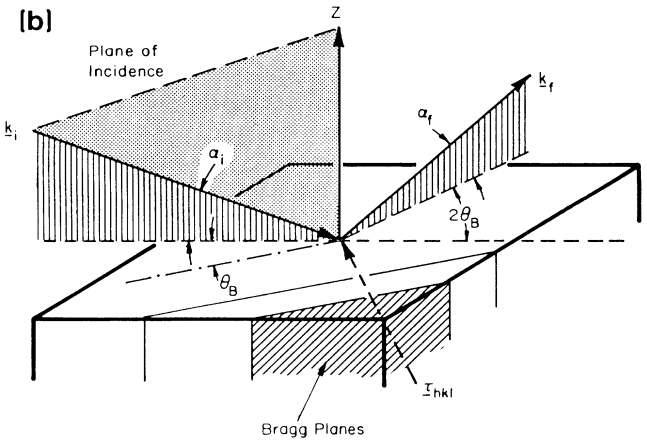

FIG. 2. Grazing incidence diffraction geometries (see the text).

situation was considered by Vineyard in introducing the DWA.) The required variability in the wavelength λ_ϕ can be provided by the continuous spectrum of synchrotron radiation facilities. In a more versatile geometry, as also used in this study, the momentum transfer Q (scattering vector) is not in the plane of incidence [Fig. 2(b)]. In this case the Bragg planes hkl lie perpendicular to the surface, accordingly, the Bragg condition is fulfilled, when $Q_{\|}=\tau_{hkl}$ ($Q_{\|}$ being the momentum transfer parallel to the surface) and the momentum transfer Q_z perpendicular to the surface disappears. It will turn out that in this geometry the incident angle α_i and the exit angle α_f can be controlled independently within the total reflection regime (see below).

In both cases the refraction correction of the momentum transfer Q_z perpendicular to the crystal surface has to be accounted for (Snell's law). Thus,

$$Q_z'=k_i^{(z)'}-k_f^{(z)'} ,$$

with

$$k_{i,f}^{(z)'}=\pm(2\pi/\lambda)(\sin^2\alpha_{i,f}-2\delta-2i\beta)^{1/2} . \quad (4)$$

[The prime denotes (in what follows) quantities inside the crystal.] The photoelectric absorption parameter $\beta=\mu\lambda/4\pi$ (μ linear absorption coefficient) has been included in Q_z' in order to bury the unphysical discontinuities which emerge in the transparent crystal at the critical angle. (The index of refraction reads then $n_\infty=1-\delta-i\beta$.) Consider now for the sake of argument the case $\beta=0$: Inspection of Eq. (4) then shows that the real part $q_z'=\mathrm{Re}(Q_z')$ of the momentum transfer vanishes, whenever α_i and α_f are less than α_c. (Note that $2\delta=\sin^2\alpha_c$.) This is, in particular, important in the scattering geometry of Fig. 2(b): Since the Bragg condition has to be fulfilled *inside* the crystal, both angles $\alpha_{i,f}$ can afford nonzero values within the total reflection regime without affecting the Bragg condition. When α_i or α_f are below α_c the imaginary part of Q_z' dominates and leads to a strong exponential damping of the transmitted wave field ("evanescent waves"). The observed scattering then originates from a depth Λ as given by $|\mathrm{Im}(Q_z')|^{-1}$ which will be called "scattering depth" in order to distinguish it from the penetration depth l^* of Eq. (2). The equivalence of grazing incidence (α_i) and grazing exit (α_f) evanescent wave fields has been verified experimentally by Becker, Golovchenko, and Patel[14] on a Ge single-crystal surface and has recently been discussed by Dietrich and Wagner[8] in the context of a grazing incidence scattering for the measurement of critical diffuse surface scattering associated with structural phase transitions.

Incidently it should be mentioned that the form of Q_z' also yields the well-known refraction correction of Bragg's law in the symmetric Bragg case. By inserting $\alpha_{i,f}=\theta_B$ into Eq. (4) the relation $\sin^2\theta_B=\sin^2\theta_B'+2\delta$ is obtained which is already discussed in the standard textbook by Compton and Allison[15] and has recently been employed to study superlattices.[16]

The calculation of Λ from Eq. (4) gives:[6]

$$\Lambda=\lambda/[2\pi(l_i+l_f)] ,$$

with

$$l_{i,f}=2^{-1/2}\{(2\delta-\sin^2\alpha_{i,f})+[(\sin^2\alpha_{i,f}-2\delta)^2+(2\beta)^2]^{1/2}\}^{1/2} . \quad (5)$$

Its dependence on α_i and α_f is illustrated in Fig. 3 for $\beta=1\times10^{-6}$ (as fulfilled in the case of an Fe_3Al crystal studied with a wavelength of $\lambda=1.5$ Å).

For $\alpha_i/\alpha_c\le1$ the maximum value of Λ is determined by the penetration depth l^* of the evanescent wave, whereas for $\alpha_i/\alpha_c>1$ the upper limit of Λ is merely determined by photoabsorption. The lower limit of Λ in the latter case is still created by evanescent waves, since $\alpha_f/\alpha_c\le1$ ("grazing exit diffraction"). We note here that for the specular beam ($\alpha_i=\alpha_f$) the common result[17]

$$l_{SB}=\lambda/[4\pi l_i] \quad (6)$$

is recovered and shown in Fig. 3 as a function of α_i/α_c. (Note the logarithmic scale.)

Any kinematic scattering intensity (I_{GID}) observed near the condition of total external reflection has the form

$$I_{GID}(Q')\propto|T_i|^2S(Q')|T_f|^2 , \quad (7)$$

where $S(Q')$ is the scattering law of the scattering process under consideration and $T_{i,f}$ are the Fresnel transmission coefficients (Fig. 1) associated with the angles $\alpha_{i,f}$. Feidenhans'l[18] has tested the validity of Eq. (7) experimentally in the particularly simple case of two-dimensional Bragg scattering: By employing the scattering geometry of Fig. 2(b), he has investigated the $\alpha_{i,f}$ dependence of the GID Bragg scattering from a InSb(111)$B3\times3$ reconstructed surface. Since the z component $S(Q_z')$ of a two-dimensional (2D) structure factor is constant ("Bragg rods"), the $\alpha_{i,f}$ dependence of $I_{GID}(Q_z')$ is only determined by the Fresnel transmissivi-

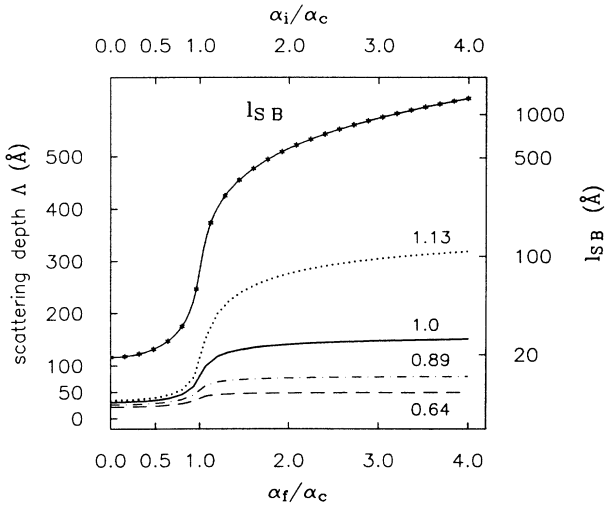

FIG. 3. Scattering depth Λ (left scale) as a function of α_f/α_c for various values $\alpha_i/\alpha_c=0.64$, 0.89, 1.0, and 1.13. The solid curve marked with asterisks shows the penetration depth l_{SB} of the specular beam as function of α_i/α_c on a logarithmic scale (right scale).

ties as observed by Feidenhans'l.

In the experiment described below we have studied the more complicated complementary case, where all illuminated near-surface layers contribute to the Bragg intensity except the first p layers ($p=1,2,\ldots$). The corresponding z component of the scattering law is then

$$S_{-p}(Q_z')=\left|\sum_{n=p}^{\infty} e^{-iQ_z' z_n}\right|^2=\frac{e^{-2pa/\Lambda}}{|1-e^{-iQ_z' a}|^2}\ , \tag{8}$$

where z_n is the z component of the basis vector R_n of unit cell n and a the lattice constant. For a discussion of $S_{-p}(Q_z')$ it is convenient to expand the exponential damping terms $\exp(-a/\Lambda)$, occurring in the denominator, up to second order in a/Λ. Then Eq. (8) reads (see Ref. 7)

$$S_{-p}(Q_z')=\frac{(\Lambda/a)^2 e^{-2pa/\Lambda}}{1+[(2\Lambda/a)\sin(q_z' a/2)]^2}\ . \tag{9}$$

In Fig. 4 $S_{-p}(Q_z')$ is calculated according to Eqs. (9) and (5) as a function of α_f/α_c for a fixed value $\alpha_i/\alpha_c=0.5$, where the two cases $p=0$ and $p=1$ are illustrated. It turns out that $S_{-p}(Q_z')$ exhibits some remarkable features.

(a) The maximum value of S_{-p} is not attained for $\alpha_f=0$, but for $\alpha_f\approx\alpha_c$. This behavior of S_{-p} can be understood as follows. Consider first the regime $\alpha_f\leq\alpha_c$, where any variation of α_f does not affect changes in the momentum transfer inside the crystal, but only a significant change in the scattering depth. Thus, $S_{-p}(Q_z')$ increases [according to Eq. (9)] proportional to $(\Lambda/a)^2\exp(-2pa/\Lambda)$. When α_f exceeds α_c, the subsequent increase of the perpendicular momentum transfer q_z' results in a gradual loss of the exact Bragg condition which then counters the action of the still increasing value of Λ. The predicted vacuum shift ΔQ_z of the maximum of the interference function from the vacuum reciprocal-lattice vector is therefore a very particular effect of the evanescent absorption associated with grazing incidence Bragg diffraction. It can be verified quite simply that for ΔQ_z the relation

$$\Delta Q_z\approx(16\pi r_e\bar{\rho}_e)^{1/2} \tag{10}$$

holds and is, accordingly, only a property of the mean electron density of the crystal and, in particular, independent of the used wavelength and the crystal structure.

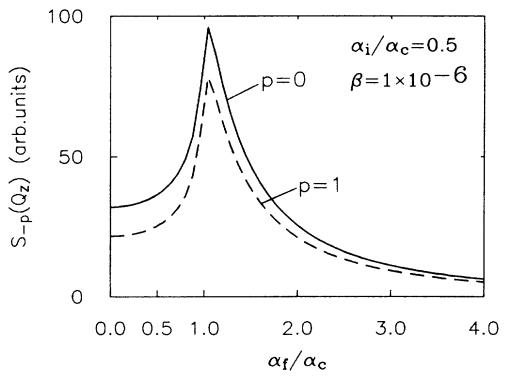

FIG. 4. Theoretical values for $S_{-p}(Q_z')$ as a function of α_f/α_c according to Eq. (9). The incident angle is assumed to be $\alpha_c/2$. The two cases $p=0$ and $p=1$ are shown (see the text).

(b) Removal of only one atomic layer from the Bragg scattering process affects crucially the GID intensity distribution in the regime of total external reflection. This demonstrates the potential of α_f-resolved GID experiments for obtaining depth-controlled structural information on near-surface atomic layers.

In the following, we will describe a GID experiment on a mosaic single-crystal surface, where the predictions by the kinematic scattering theory [as expressed in Eqs. (9) and (10)] will be tested.

EXPERIMENTAL DETAILS

Since kinematic Bragg scattering is proportional to the number of atomic layers involved, the ratio of GID Bragg intensity to bulk Bragg intensity is proportional to $(\mu\Lambda)$ and, thus, only of the order of 10^{-4}. Due to this severe intensity problem, the observation of Bragg scattering with simultaneous total external reflection has not been feasible until the availability of the highly brilliant synchrotron radiation.

In this experiment the scattering geometry of Fig. 2(b) was realized. Figure 5 depicts the schematic setup of a GID experiment performed at the Al station of Cornell High Energy Synchrotron Source (CHESS) which is supplied with the continuous radiation from a six-pole wiggler. With a focusing Si(111) monochromator, the x-ray wavelength $\lambda=1.5$ Å was singled out together with its higher harmonics which were suppressed by the subsequent total external reflection mirror. Through examples we have studied the (222) Bragg reflection excited under total external reflection from a Fe_3Al single-crystal surface [its crystallographic orientation being $(\bar{1}10)$]. The sample was mounted horizontally on a two-circle diffractometer which allowed the control of the exact (horizontal) Bragg condition $Q_{||}=\tau(222)$ through the θ and 2θ circle. For the adjustment of the incidence angle α_i the entire diffractometer was rotated by a (stepping motor controlled) optical bench with an accuracy of ±0.1 mrad. The actual values α_i were monitored most simply by the momentary direction of the specular beam (its intensity was also registered by an ionization chamber). The use of a position-sensitive detector (PSD) (Ref. 19) provided an elegant performance of the α_f scan of the totally reflected scattering. The size and divergence of the incident x-ray beam have to be addressed in further detail. Since the penetration depth of the evanescent wave field depends most sensitively on the incidence angle α_i, this experimental parameter has to be extremely well defined. Therefore, synchrotron radiation is, because of its "natural" minute vertical beam divergence (typically 0.1 mrad), an outstanding x-ray source for this kind of experiment.[20] With our sample surface being a 15 mm×15 mm square, only 150 μm of the vertical linear extension of the x-ray beam contributes to the signal (for grazing angles between 0 and 10 mrad). Since any excess beam height would only increase the background scattering, the incident x-ray beam was narrowed by vertical slits to 150 μm, whereas the horizontal slits were relaxed to some 4 mm. A horizontal

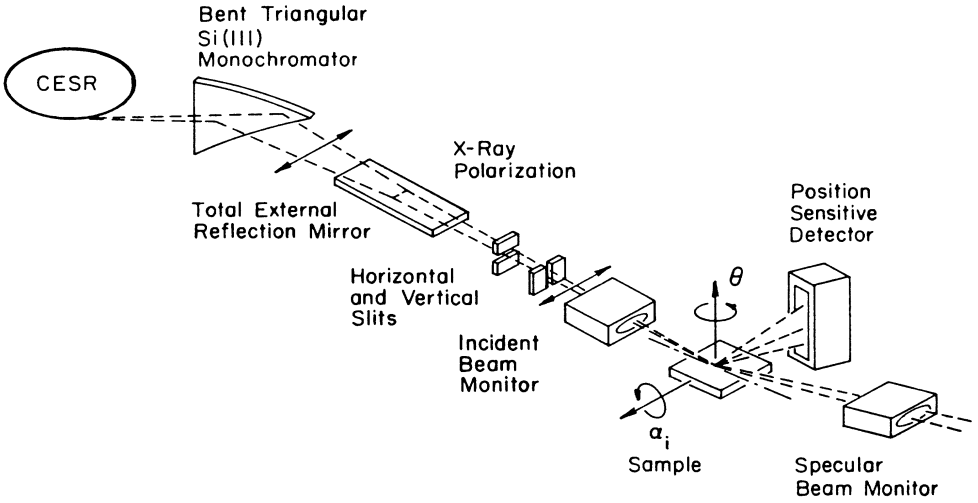

FIG. 5. Schematic setup of a synchrotron GID experiment.

beam divergence of 0.35° ensured a reliable integration of the Bragg intensity parallel to the crystal surface. (The mosaic spread of the crystal was measured to be 0.10°.)

We want to draw the readers attention to the polarization of the x-ray beam which is in this experimental setup perpendicular to the plane of incidence (see Fig. 5). Therefore, any GID intensity scattered out of the plane of incidence is affected by the polarization factor $\cos^2(2\theta_B)$, which thus renders GID Bragg reflections associated with Bragg angles close to 45° inaccessible to the experiment. This is one of the major drawbacks of this experimental arrangement and can be avoided in the geometry shown in Fig. 2(a).

EXPERIMENTAL RESULTS AND DISCUSSION

The unit cell of Fe_3Al associated with a lattice parameter $a_0=5.78$ Å contains twelve Fe and four Al atoms which results in a critical angle of $\alpha_c=6.2$ mrad and a Bragg angle of $\theta_B=26.7°$ for the (222) reflection (with $\lambda=1.5$ Å).

If the angle θ of the sample is *not* set to fulfill the Bragg condition $\theta=\theta_B(222)$, then the diffuse scattering from the sample surface (Compton and temperature diffuse scattering) can be studied: Figure 6 shows, as a typical result, the diffuse surface scattering observed at $2\theta_B=53.4°$ for $\alpha_i\approx\alpha_c$. The shown α_f dependence of the scattering between 0 and 25 mrad has been recorded with the PSD. Since the range of the vertical (α_f) scan is very small in reciprocal space, $\Delta Q_z=(2\pi/\lambda)\Lambda\alpha_f=0.1$ Å^{-1}, the slowly varying scattering phase of the temperature diffuse scattering contribution can be assumed constant, therefore the underlying structure factor of the observed diffuse scattering is simply proportional to the number of atomic layers contributing, as for the Compton incoherent scattering.[21] Thus, $S_{\rm dif}(\alpha_f)\propto\Lambda$, and, according to Eq. (7), we conclude that the associated scattering intensity $I_{\rm dif}$ should follow the simple law

$$I_{\rm dif}(\alpha_f)\propto\Lambda\,|\,T_f\,|^2\,. \tag{11}$$

Taking $|\,T_f\,|^2$ from Fig. 1 (dashed line) and Λ from Eq. (5), this relation yields the solid line in Fig. 6 for the diffuse intensity distribution which is readily observed.[22]

By rotating the (222) surface net planes into reflection condition, totally reflected Bragg intensity is scattered into the position-sensitive detector, where its α_f dependence is analyzed. We have studied the shape of the Bragg intensity essentially for three different incidence angles $\alpha_i/\alpha_c=0.64$, 0.89, and 1.1 and have observed integrated counting rates of typically 100 counts/sec. Given that the primary intensity (I_0) at the sample is of the order of 10^{10} counts/sec, we find that the GID Bragg reflectivity is approximately 10^{-8}. An estimation based on kinematic scattering theory[21] gives values between 10^{-7} and 10^{-8} for the reflection power depending on the assumptions on the effective surface area. We consider this agreement between the measured and calculated kinematic GID reflection power as evidence that a further kinematic treatment of the observed Bragg scattering is appropriate. Note that, according to Cowan,[10] strong

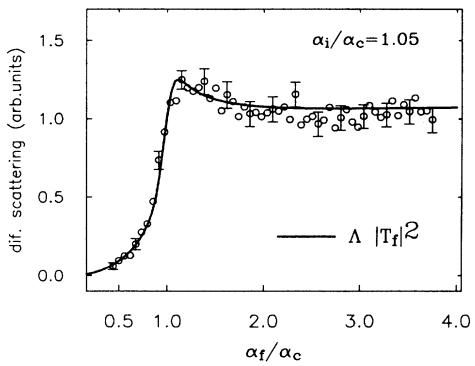

FIG. 6. Diffuse surface scattering from the Fe_3Al ($\bar{1}10$) surface as a function of α_f/α_c observed at $\alpha_i/\alpha_c=1.05$ and $2\theta_B=53.4°$ (open symbols). The solid line is calculated according to Eq. (13) and is normalized to the experimental intensity maximum at the critical angle.

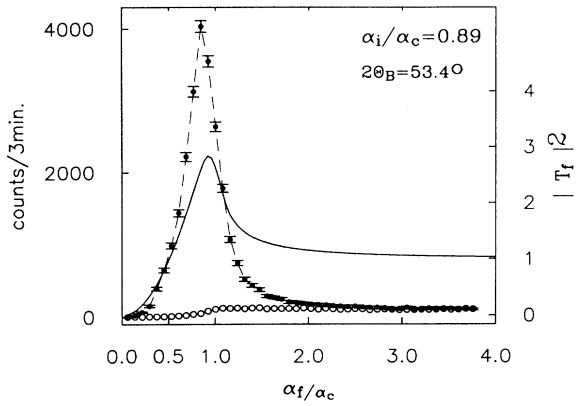

FIG. 7. Raw data as a function of α_f/α_c obtained at $\alpha_i/\alpha_c=0.89$: The solid symbols show the data observed in Bragg condition for the (222) surface reflection, whereas the open symbols show the data recorded after a θ rotation of the sample by 5° (see Fig. 5). The solid line shows the Fresnel transmissivity (right scale) associated with the scattering geometry.

multiple-scattering effects (out of the plane of incidence) would render the GID Bragg scattering as strong as roughly one-third of the specular beam intensity.

Figure 7 shows, an an illustrating example, the raw data obtained for $\alpha_i/\alpha_c=0.89$. The Bragg scattering as well as the diffuse scattering background are proportional to $|T_f|^2$ which is also shown as the solid line. The following treatment of data has been applied.

After subtraction of the diffuse scattering background, the experimental points were normalized to the effective primary intensity intercepted by the sample, which is $(I_0|T_i|^2/\sin\alpha_i)$. The final experimental results for $S_{-p}(Q_z')$ follow from that after correction for the Fresnel transmissivity of the interface. They are shown in Fig. 8 for the three different incidence angles. Due to the small transmission of the interface for $\alpha_f<2.0$ mrad, the experimental data become increasingly unreliable in this regime. In addition, we found through the analysis of the specular intensity that noticeable absorption effects occurred at angles $\alpha_f\leq 2.5$ mrad which we referred to surface roughness. Therefore, we have excluded the exit angle range from 0 to 2.5 mrad from the further discussion.

The prominent feature of the observed interference functions is their peak structure centered at $\alpha_f/\alpha_c\sim 1$ which confirms the predictions expressed in Eq. (10). Since the origin of this peak is due to the action of the varying scattering depth Λ, we can conclude that the data shown represent a depth profile of the GID Bragg intensity. The solid lines in Fig. 8 are calculated according to Eq. (9) and are in good agreement with the experimental data points.[22] Deviations of the measured scattering law from the calculated one emerge essentially in the region $\alpha_f\ll\alpha_c$. One way of settling this discrepancy is, according to Fig. 3, by assuming that the first atomic layers do not contribute to the Bragg intensity. Possible reasons for this can be found in the presence of oxide layers and in the onset of absorption effects due to surface roughness. The dashed lines in Fig. 8 are the result of a calculation of

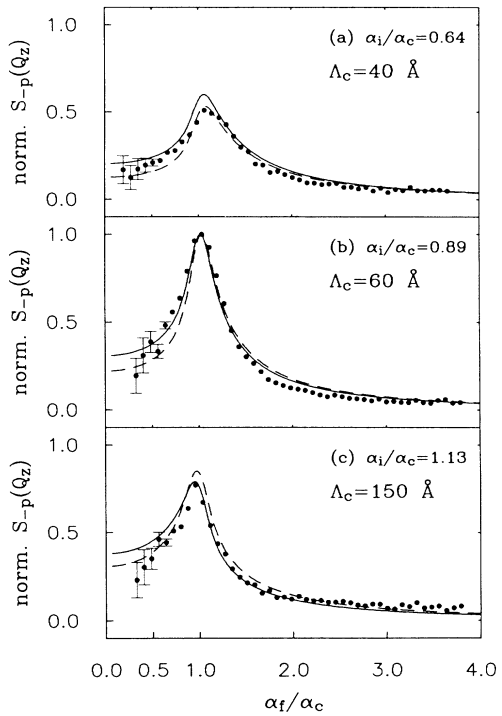

FIG. 8. Final experimental results of $S_{-p}(Q_z')$ at three different incidence angles $\alpha_i/\alpha_c=0.64$, 0.89, and 1.13 (solid symbols) compared with calculations according to Eq. (9) assuming $p=0$ (solid line) and $p=2$ (dashed line). The "critical scattering depth" Λ_c indicated for each scan gives the scattering depth at $\alpha_f/\alpha_c=1$. All data are normalized to the maximum value in (b).

Eq. (9) assuming that $p=2$ and give indeed a slight improvement in the fit. We want to point out that all scattering distributions shown in Fig. 8 are normalized to the maximum in the interference function associated with $\alpha_i/\alpha_c=0.89$. Therefore, in this representation of the data, the removal of the top layers from the Bragg scattering process does not show up in a distinct intensity decrease in the vicinity of the critical angle (as illustrated in Fig. 3), but merely in a change in the peak shape.

In conclusion, we have shown that the kinematic scattering theory based on the DWA is appropriate to describe Bragg scattering excited under the conditions of total external reflection from a mosaic crystal surface. Our analysis made evident that the absorption phenomena associated with the scattering under grazing angles have to be considered carefully and can provide the potential for attaining a depth profile of the structure of near-surface atomic layers.

ACKNOWLEDGMENTS

I am grateful to B. W. Batterman for his encouragement and for many clarifying discussions and to Dan Wack for the pleasant collaboration, as well as to R. Feidenhans'l for correspondence. The work was supported by the Alexander von Humboldt Foundation (Bonn, West Germany) and by the National Science Foundation (NSF) through Grant Nos. DMR-84-12465 and DMR-85-43513.

*Present address: Sektion Physik, Universität München, Geschwister-Scholl Platz 1, D-8000 Muenchen 22, West Germany.

[1]W. C. Marra, P. Eisenberger, and A. Y. Cho, J. Appl. Phys. **50**, 6927 (1979).

[2]R. J. Comstock, J. B. Cohen, and H. R. Harrison, Acta. Metall. **33**, 423 (1985).

[3]I. K. Robinson, Phys. Rev. Lett. **50**, 1145 (1983).

[4]J. Bohr, R. Feidenhans'l, M. Nielsen, and M. Toney, Phys. Rev. Lett. **54**, 1275 (1985).

[5]M. Nielsen, Z. Phys. B **61**, 415 (1985).

[6]H. Dosch, B. W. Batterman, and D. C. Wack, Phys. Rev. Lett. **56**, 1144 (1986).

[7]G. H. Vineyard, Phys. Rev. B **26**, 4146 (1982).

[8]S. Dietrich and H. Wagner, Phys. Rev. Lett. **51**, 1469 (1983).

[9]S. Dietrich and H. Wagner, Z. Phys. B **56**, 207 (1984).

[10]P. L. Cowan, Phys. Rev. B **32**, 5437 (1985).

[11]A. M. Afans'ev and M. K. Melkonyan, Acta Crystallogr. A **39**, 207 (1983).

[12]M. Born and E. Wolf, *Principles of Optics* (Pergamon, Oxford, 1970).

[13]With nonzero photoabsorption the transmissivity of Eq. (3) reads $T=\{2\sin\alpha/[(\sin\alpha+c_1)^2+c_2^2]\}[(\sin\alpha+c_1)+ic_2]$ with $c_{1,2}=2^{-1/2}\{\pm(\sin^2\alpha-2\delta)+[(\sin^2\alpha-2\delta)^2+4\beta^2]^{1/2}\}^{1/2}$. The parameter β is defined as $\mu\lambda/4\pi$.

[14]R. S. Becker, J. A. Golovchenko, and J. R. Patel, Phys. Rev. Lett. **50**, 153 (1983).

[15]A. H. Compton and S. K. Allison, *X-rays in Theory and Experiment* (Nostrand, New York, 1935).

[16]P. F. Miceli, D. A. Neumann, and H. Zabel, Appl. Phys. Lett. **48**, 24 (1986).

[17]L. G. Parratt, Phys. Rev. **95**, 359 (1954).

[18]R. Feidenhans'l (private communication).

[19]The PSD system that was used was a metal wire in a Xe atmosphere; its spatial resolution was $\Delta s=200\ \mu$m.

[20]Due to the Wiggler-field-induced shift in the critical energy the actual vertical divergence was slightly increased in our experiment to $\Delta\alpha_i=0.4$ mrad.

[21]B. E. Warren, *X-ray diffraction* (Addison-Wesley, Reading, Mass., 1969).

[22]The calculations include the vertical beam divergence $\Delta\alpha_i=0.4$ mrad as well as the spatial resolution of the PSD (giving $\Delta\alpha_f=0.44$ mrad).